
Spatiotemporal Residual Regularization with Dynamic Mixtures for Traffic Forecasting

Seongjin Choi^{1,2} Nicolas Saunier^{3,2} Martin Trepanier^{4,2} Lijun Sun^{1,2}

Abstract

Existing deep learning-based traffic forecasting models are mainly trained with MSE (or MAE) as the loss function, assuming that residuals/errors follow independent and isotropic Gaussian (or Laplacian) distribution for simplicity. However, this assumption rarely holds for real-world traffic forecasting tasks, where the unexplained residuals are often correlated in both space and time. In this study, we propose Spatiotemporal Residual Regularization by modeling residuals with a dynamic (e.g., time-varying) mixture of zero-mean multivariate Gaussian distribution with learnable spatiotemporal covariance matrices. This approach allows us to directly capture spatiotemporally correlated residuals. For scalability, we model the spatiotemporal covariance for each mixture component using a Kronecker product structure, which significantly reduces the number of parameters and computation complexity. We evaluate the performance of the proposed method on a traffic speed forecasting task. Our results show that, by properly modeling residual distribution, the proposed method not only improves the model performance but also provides interpretable structures.

1. Introduction

Traffic forecasting is one of the most studied topics in transportation engineering. The objective of traffic forecasting is to predict future traffic states based on historical

observations. Reliable and accurate traffic forecasting is a critical component of intelligent transportation systems (ITS), including both Advanced Traffic Management Systems (ATMS) and Advanced Traveler Information Systems (ATIS). Traffic management centers can proactively apply proper traffic controls to transportation networks to mitigate congestion and increase overall efficiency. For example, predicted traffic states are used for reinforcement learning-based traffic signal control (Kim & Jeong, 2019). On the other hand, individual users can use future traffic states to plan their trips and choose proper routes. For instance, visualizations of traffic state are provided for the users to explore both real-time and predicted spatiotemporal congestion patterns on a selected route (Lee et al., 2019).

The unprecedented availability of traffic data and significant advancements in data-driven algorithms have sparked considerable interest and developments in traffic forecasting. In particular, state-of-the-art deep learning models such as DCRNN (Li et al., 2017), STGCN (Yu et al., 2017), GraphWavenet (Wu et al., 2019), and Traffic Transformer (Cai et al., 2020), have demonstrated superior performance for traffic speed forecasting over classical methods. Deep learning approaches have shown clear advantages in capturing complex non-linear relationships in traffic forecasting; for example, in the aforementioned models, Graph Neural Networks (GNNs), Recurrent Neural Networks (RNNs), Gated Convolutional Neural Networks (Gated-CNNs), and Transformer are employed to capture spatiotemporal patterns in traffic data (Li et al., 2015; Zhao et al., 2019; Cui et al., 2019; Liu et al., 2022).

When training DNN-based models, conventional loss functions include Mean Squared Error (MSE) and Mean Absolute Error (MAE). This convention of using MSE or MAE is based on the assumption that the residuals, or the deviation between the predicted value and the target value, follow either independent Gaussian distribution or Laplacian distribution. If the errors are assumed to be isotropic white noises, the Maximum Likelihood Estimation (MLE) corresponds to minimizing the MSE. Likewise, the MLE corresponds to minimizing MAE if the errors are assumed to follow an isotropic zero-mean Laplacian distribution. However, the assumption of having uncorrelated and independent resid-

¹Department of Civil Engineering, McGill University, 817 Sherbrooke Street West, Montreal, Quebec, H3A 0C3, Canada

²Interuniversity Research Centre on Enterprise Networks, Logistics and Transportation (CIRRELT) ³Department of Civil, Geological and Mining Engineering, Polytechnique Montreal, 2500, chemin de Polytechnique, Montreal, Québec, H3T 1J4, Canada

⁴Department of Mathematics and Industrial Engineering, Polytechnique Montreal, 2500, chemin de Polytechnique, Montreal, Québec, H3T 1J4, Canada.

Correspondence to: Lijun Sun <lijun.sun@mcgill.ca>.

uals does not hold in many real-world applications. This is particularly the case for spatiotemporal forecasting tasks, where spatiotemporally correlated errors are prevalent due to measurement errors, the ignorance of other influential variables, and model misspecification (Sun et al., 2021). For instance, considering that weather conditions have a substantial impact on traffic speed, any DNN-based forecasting model that ignores these external factors will result in autocorrelated residuals.

Recent studies, however, have presented clear evidence that the above-stated conventional assumption often fails to hold. For example, (Sun et al., 2021) claimed that in most cases, prediction errors of time series prediction models are actually autocorrelated due to the temporal nature of the data. Also, (Kim et al., 2022) analyzed the errors in the traffic forecasting models and found that the errors are correlated in both spatial and temporal dimensions. Moreover, (Zambon & Alippi, 2022) proposed the AZ-whiteness test to find spatial and temporal dependencies in a spatiotemporal graph and reported that the prediction result of all of the baseline models such as DCRNN, GatedGN (Satorras et al., 2022), and Graph-Wavenet were actually correlated in both spatial and temporal dimension.

Only a few studies proposed methodologies or tricks to correct the spatiotemporally correlated residuals. (Sun et al., 2021) proposed a method to adjust the autocorrelated errors by assuming first-order correlation in the temporal dimension. However, the focus of this study was on general time-series forecasting, so there was less attention to the spatially correlated errors. (Kim et al., 2022) proposed ResCAL, a residual estimation module, which calibrates the forecasting result by estimating future residuals using previous observations of residuals as well as the graph signal. (Cho et al., 2022) proposed a regularization method called WaveBound, which estimates the proper error bounds of training loss for both spatial and temporal dimensions by introducing a target network that is updated using an exponential moving average. The target network is then used as a reference for the source network and guide a reasonable level of training loss to the source network.

In this study, we propose a novel approach to model spatiotemporally *correlated* residuals to enhance DNN-based traffic forecasting models. Most of the previous studies focus on correcting or adjusting the output value by assuming first-order autocorrelation or using other neural networks to predict the spatiotemporally correlated residuals. However, these studies do not explicitly consider the likelihood function in the training process. In this study, we propose to train the model by redesigning the model as a probabilistic forecasting model, and we train a given forecasting model explicitly with the likelihood function. We use a dynamic (e.g., time-varying) mixture of Gaussian distributions as a

flexible structure to characterize the spatiotemporal residuals in multistep-ahead forecasting. Then, we train the model by maximizing the likelihood of the residual distribution as well as conventional MSE/MAE loss. The fundamental challenge in this approach is the high computational cost due to the large $NT \times NT$ spatiotemporal covariance matrix for the residual process, where N is the number of sensors and T is the number of timesteps to forecast. For model scalability, we design a decomposition technique that reparameterizes the covariance in each mixture component as a Kronecker product of two separate spatial and temporal covariance matrices. In addition, we parameterize these covariances using the Cholesky factorization of the precision matrices (inverse of the covariance matrix) to further reduce the computational complexity in model training. We name this approach *SpatioTemporal Residual Regularization (STRR)* and use it as an auxiliary loss to train the model with conventional MSE or MAE loss.

2. Methodology

2.1. Background

First, we briefly give out the formulation of the problem, i.e., short-term traffic speed forecasting. Given a time window t , we denote by v_t^n the average speeds of the n -th sensor. The speed observations in the whole network at the given time window are denoted by vector $\mathbf{x}_t = [v_t^1, v_t^2, \dots, v_t^N]^T \in \mathbb{R}^N$. Given the K historical observations $X_t = [\mathbf{x}_{t-K+1}, \dots, \mathbf{x}_t] \in \mathbb{R}^{N \times K}$, we aim to predict the speed of N sensors for the next T steps, i.e., $Y_t \in \mathbb{R}^{N \times T}$ as a spatiotemporal speed matrix.

Conventional training of deep-learning models for short-term traffic speed forecasting problem can be regarded as learning of a mean-prediction function f_M by minimizing MSE or MAE loss ($\mathcal{L}_{MSE/MAE}$) as follows:

$$f_M^* = \arg \min_{f_M} \mathcal{L}_{MSE/MAE}$$

$$\mathcal{L}_{MSE/MAE} = \begin{cases} \|Y_t - M_t\|_F^2 & \text{for MSE,} \\ \|Y_t - M_t\|_1 & \text{for MAE,} \end{cases} \quad (1)$$

where $M_t = f_M(X_t) \in \mathbb{R}^{N \times T}$ is a matrix of the expected future traffic speed.

The convention of using MSE loss for training deep learning models for traffic speed forecasting assumes that the residual process, $R_t = Y_t - M_t \in \mathbb{R}^{N \times T}$, follows a zero-mean Gaussian distribution with isotropic noise:

$$\text{vec}(R_t) \sim \mathcal{N}(0, \Sigma = \sigma^2 I), \quad (2)$$

where $\text{vec}(R_t) \in \mathbb{R}^{NT}$ is a vectorized form of R_t , and Σ is the covariance matrix, and σ is the fixed standard deviation.

2.2. Spatiotemporal Residual Regularization with Kronecker Product Structure

In this study, we propose a Spatiotemporal Residual Regularization (STRR) to improve the performance of conventional deep-learning models for short-term traffic speed forecasting by redesigning the loss function.

We tackle that the residuals are actually spatiotemporally correlated, and the simple assumption in Eq. (2) is too restrictive and often fails to hold for real-world data. To address this issue, we assume that the residual process, R_t , follows a certain distribution and directly train the model by using maximum likelihood as follows:

$$\begin{aligned} \mathcal{L} &= \mathcal{L}_{MSE/MAE} + \rho \mathcal{L}_{STRR}, \\ \mathcal{L}_{STRR} &= -\log p(R_t), \end{aligned} \quad (3)$$

where \mathcal{L}_{STRR} is the SpatioTemporal Residual Regularization loss (i.e., the negative log-likelihood of the residuals), $p(R_t)$ is the probability density of the assumed distribution of the residuals, and ρ is the regularization parameter.

One intuitive and interpretable solution to model a complex multivariate distribution is to use a *mixture of Multivariate Gaussian distributions*. The idea behind using the mixture of Gaussian distribution is that this approach can represent or approximate practically any distribution of interest while staying intuitive and easy to handle (Hara et al., 2018). Furthermore, we use a *dynamic mixture of multivariate zero-mean Gaussian distribution* to model the distribution of spatiotemporally correlated residuals and assume that the probability density function of $p(R_t)$ can be formulated as a mixture of K multivariate zero-mean Gaussian with dynamic (i.e., time-varying) mixture weights ω_t^k as follows:

$$R_t \sim \sum_{k=1}^K \omega_t^k \cdot \mathcal{N}(0, \Sigma^k), \quad \forall t, \quad (4)$$

where $\Sigma^k \in \mathbb{R}^{NT \times NT}$ is the spatiotemporal covariance matrix for k -th component, and $\omega_t^k \geq 0$ is the time-varying weight (proportion) for k -th covariance matrix, which should be sum to 1 ($\sum_{k=1}^K \omega_t^k = 1$) for any t . Here, note that the mixture weight, ω_t^k , is time-dependent (or input-dependent; $\omega_t^k = f_\omega(X_t)$), while the covariance matrix in the component distribution Σ^k is not. This representation allows modeling the time-varying distribution of residual distribution while remaining intuitive and interpretable by analyzing the component distribution.

Although simple, this approach has a critical issue in computing the log-likelihood of this distribution, which requires high computation cost due to the large size of Σ^k (i.e., $NT \times NT$). Directly learning such a large spatiotemporal covariance matrix ($\Sigma^k \in \mathbb{R}^{NT \times NT}$) is infeasible if N or T becomes large since computing the negative log-likelihood

involves calculating the inverse and the determinant of the covariance matrix. For example, PEMS-BAY data, which is one of the widely used traffic speed datasets, consists of observations from 325 sensors, and the prediction horizon is usually set to 1 hour (i.e., 12 timesteps with a 5-minute interval). This would result in $N = 325$ and $T = 12$, and the size of Σ^k becomes 3900×3900 .

Instead of training such a large matrix in an inefficient way, we propose a decomposition method to address the scalability issue. Our key idea is to parameterize each spatiotemporal covariance matrix (Σ^k) as a Kronecker product of spatial covariance matrix (Σ_S^k) and temporal covariance matrix (Σ_T^k) as follows:

$$R_t \sim \sum_{k=1}^K \omega_t^k \cdot \mathcal{N}(0, \Sigma^k = \Sigma_T^k \otimes \Sigma_S^k), \quad \forall t, \quad (5)$$

where $\Sigma_S^k \in \mathbb{R}^{N \times N}$ and $\Sigma_T^k \in \mathbb{R}^{T \times T}$ are spatial and temporal covariance for k -th component, respectively. The Kronecker product of two matrices $P \in \mathbb{R}^{A \times B}$ and $Q \in \mathbb{R}^{C \times D}$ is the block matrix size of $AB \times CD$ as follows:

$$P \otimes Q = \begin{bmatrix} p_{11}Q & p_{12}Q & \cdots & p_{1b}Q \\ p_{21}Q & p_{22}Q & \cdots & p_{2b}Q \\ \vdots & \vdots & \ddots & \vdots \\ p_{a1}Q & p_{a2}Q & \cdots & p_{ab}Q \end{bmatrix}. \quad (6)$$

This representation is equivalent to assuming the residual (R_t) follows a dynamic mixture of matrix normal distribution with zero-mean as follows:

$$R_t \sim \sum_{k=1}^K \omega_t^k \cdot \mathcal{MN}(0, \Sigma_S^k, \Sigma_T^k), \quad \forall t, \quad (7)$$

where the probability density function for the random matrix $X \in \mathbb{R}^{P \times Q}$ that follows a matrix normal distribution $\mathcal{MN}(M, U, V)$ with density

$$\begin{aligned} p_{MN}(X|M, U, V) &= \frac{\exp\left(-\frac{1}{2} \text{Tr}[V^{-1}(X-M)^T U^{-1}(X-M)]\right)}{(2\pi)^{PQ/2} |V|^{P/2} |U|^{Q/2}}. \end{aligned} \quad (8)$$

Then, the STRR loss can be calculated as follows:

$$\begin{aligned}
 \mathcal{L}_{STRR} &= -\log p(R_t) = \log \sum_{k=1}^K \omega_t^k \cdot p_{MN}(R_t|0, \Sigma_S^k, \Sigma_T^k) \\
 &= \log \sum_{k=1}^K \exp \left(\log \omega_t^k - \frac{NT}{2} \log(2\pi) \right. \\
 &\quad \left. - \frac{N}{2} \log(|\Sigma_T^k|) - \frac{T}{2} \log(|\Sigma_S^k|) \right. \\
 &\quad \left. - \frac{1}{2} \text{Tr} [(\Sigma_T^k)^{-1} (R_t)^\top (\Sigma_S^k)^{-1} (R_t)] \right). \tag{9}
 \end{aligned}$$

For ease of computation, we further parameterize Σ_S^k and Σ_T^k using the Cholesky factorization of the precision (inverse of covariance) matrices, Λ_S^k and Λ_T^k , as follows:

$$\begin{aligned}
 (\Sigma_S^k)^{-1} &= \Lambda_S^k = (L_S^k) (L_S^k)^\top, \\
 (\Sigma_T^k)^{-1} &= \Lambda_T^k = (L_T^k) (L_T^k)^\top,
 \end{aligned} \tag{10}$$

where L_S^k and L_T^k are the k -th spatial and temporal lower triangular matrices, respectively.

Also, note that training a matrix does not guarantee the *invertibility* of a matrix. During implementation, we found that parameterizing with covariance matrices can result in divergence of the loss function, gradient exploding, and singular (non-invertible) covariance matrix. We resolved these issues by parameterizing the precision matrix. Since we do not have to invert the matrix during training, the training process is much more stable than parameterizing the covariance matrix using Cholesky factorization. As a result, we can avoid computing inverse operations during the training and efficiently compute the determinant by summing the logarithms of diagonal entries as follows:

$$\begin{aligned}
 \Lambda_S^k &= (L_S^k) (L_S^k)^\top, \quad \Lambda_T^k = (L_T^k) (L_T^k)^\top, \\
 \log |\Lambda_S^k|^{\frac{1}{2}} &= \sum_{n=1}^N \log [L_S^k]_{n,n}, \\
 \log |\Lambda_T^k|^{\frac{1}{2}} &= \sum_{m=1}^T \log [L_T^k]_{m,m}.
 \end{aligned} \tag{11}$$

Also, the trace term can be simplified into computing the square of Frobenius Norm of $Q_t^k = (L_S^k)^\top E_t^k (L_T^k)$ as

shown in Eq. (12):

$$\begin{aligned}
 &\text{Tr} \left[\Lambda_T^k (E_t^k)^\top \Lambda_S^k E_t^k \right] \\
 &= \text{Tr} \left[(L_T^k) (L_T^k)^\top (E_t^k)^\top (L_S^k) (L_S^k)^\top E_t^k \right] \\
 &= \text{Tr} \left[(L_S^k)^\top E_t^k (L_T^k) (L_T^k)^\top (E_t^k)^\top (L_S^k) \right] \\
 &= \text{Tr} \left[\left((L_S^k)^\top E_t^k (L_T^k) \right) \left((L_S^k)^\top E_t^k (L_T^k) \right)^\top \right] \\
 &= \text{Tr} \left[(Q_t^k) (Q_t^k)^\top \right] \\
 &= \|Q_t^k\|_F^2.
 \end{aligned} \tag{12}$$

Finally, Eq. (9) can be simplified as

$$\begin{aligned}
 \mathcal{L}_{STRR} &= \log \sum_{k=1}^K \exp \left(\log \omega_t^k - \frac{NT}{2} \log(2\pi) + N \sum_{m=1}^T \log [L_T^k]_{m,m} \right. \\
 &\quad \left. + T \sum_{n=1}^N \log [L_S^k]_{n,n} - \frac{1}{2} \|Q_t^k\|_F^2 \right),
 \end{aligned} \tag{13}$$

where $Q_t^k = (L_T^k)^\top E_t^k (L_S^k)$.

Note the term inside *exponential function* may become very large (either negative or positive), and this will make it infeasible to compute the log-likelihood. To avoid numerical problems in the training process, we use Log-Sum-Exp trick $\log \sum_{n=1}^N \exp(z_n) = z^* + \log \sum_{n=1}^N \exp(z_n - z^*)$ with $z^* = \max\{z_1, \dots, z_N\}$.

Finally, we can train a given baseline model based on Eq. (3) by using both conventional MSE/MAE loss ($\mathcal{L}_{MSE/MAE}$) as well as the STRR loss (\mathcal{L}_{STRR}). We jointly train f_M , f_ω , L_T^k , and L_S^k by minimizing the total loss ($\mathcal{L} = \mathcal{L}_{MSE/MAE} + \rho \mathcal{L}_{STRR}$). Both f_M and f_ω are represented as a neural network. We slightly change the last layer of the baseline model to output a hidden representation of the given input, and we use two separate Multi-layer Perceptron (MLP) for f_M and f_ω . In other words, the baseline model is a shared layer for f_M and f_ω to calculate a hidden representation of the input, and the last MLP is the function-specific module to calculate the desired output. We do not have an activation function at the last layer of MLP for f_M since we usually use z-score normalization before feeding the input to the model, but we apply the softmax function at the last layer of MLP for f_ω to force it to be summed to 1. The gradient updates of L_T^k and L_S^k are only applied to the “lower” part of the matrices, and the values in the upper parts remain as 0 during the whole process.

Table 1. Summary of results. The best result at each column is bolded with a star mark

| Data | Model | Base Loss | RMSE | | | | MAPE | | | | MAE | | | |
|----------|----------|-----------|--------------|--------------|--------------|--------------|--------------|--------------|--------------|---------------|--------------|--------------|--------------|--------------|
| | | | 15min | 30min | 45min | 60min | 15min | 30min | 45min | 60min | 15min | 30min | 45min | 60min |
| PEMS-BAY | GWN | MSE | 2.57 | 3.36 | 3.76 | 4.05 | 2.86 | 3.81 | 4.36 | 4.75 | 1.39 | 1.76 | 1.98 | 2.15 |
| | +STRR(1) | MSE | 2.56 | 3.40 | 3.79 | 4.02 | 2.88 | 3.87 | 4.37 | 4.71 | 1.35 | 1.70 | 1.88 | 2.01 |
| | +STRR(2) | MSE | *2.54 | 3.34 | 3.69 | *3.88 | *2.83 | 3.79 | 4.25 | 4.55 | *1.34 | *1.68 | 1.86 | *1.97 |
| | +STRR(3) | MSE | *2.54 | *3.32 | *3.68 | *3.88 | *2.83 | 3.77 | 4.27 | 4.61 | *1.34 | *1.68 | *1.85 | *1.97 |
| | +STRR(5) | MSE | 2.55 | 3.34 | 3.71 | 3.92 | 2.85 | *3.73 | *4.21 | *4.50 | 1.35 | 1.68 | 1.86 | 1.98 |
| | GWN | MAE | 2.65 | 3.46 | 3.87 | 4.20 | 2.82 | 3.80 | 4.38 | 4.81 | 1.36 | 1.72 | 1.93 | 2.10 |
| | +STRR(1) | MAE | 2.53 | 3.33 | 3.70 | 3.89 | 2.83 | 3.76 | 4.25 | 4.56 | 1.35 | 1.70 | 1.87 | 1.99 |
| | +STRR(2) | MAE | *2.52 | 3.29 | 3.68 | 3.92 | 2.80 | 3.72 | 4.24 | 4.62 | 1.33 | *1.66 | 1.85 | 1.99 |
| | +STRR(3) | MAE | *2.52 | *3.28 | *3.65 | *3.88 | *2.76 | *3.69 | 4.21 | 4.56 | *1.32 | *1.66 | *1.84 | *1.97 |
| | +STRR(5) | MAE | 2.53 | 3.32 | 3.70 | 3.91 | 2.76 | 3.68 | *4.17 | *4.52 | 1.34 | 1.68 | 1.87 | 1.99 |
| METR-LA | GWN | MSE | 5.05 | 5.90 | 6.44 | 6.85 | 7.47 | 9.01 | 10.02 | 10.78 | 2.90 | 3.36 | 3.68 | 3.93 |
| | +STRR(1) | MSE | 4.95 | 5.94 | 6.53 | 6.88 | 7.16 | 8.77 | 9.76 | 10.44 | 2.84 | 3.32 | 3.65 | *3.87 |
| | +STRR(2) | MSE | 4.94 | 5.93 | 6.52 | 6.95 | *7.13 | *8.68 | 9.69 | 10.39 | *2.81 | *3.30 | *3.62 | 3.89 |
| | +STRR(3) | MSE | 4.97 | 5.95 | 6.52 | 6.92 | 7.14 | 8.72 | *9.66 | *10.32 | 2.84 | 3.34 | 3.65 | 3.91 |
| | +STRR(5) | MSE | *4.93 | *5.85 | *6.42 | *6.81 | 7.26 | 8.81 | 9.87 | 10.71 | 2.86 | 3.34 | 3.65 | 3.93 |
| | GWN | MAE | 5.12 | 6.05 | 6.66 | 7.16 | 7.21 | 8.60 | 9.47 | *10.17 | *2.78 | *3.21 | *3.51 | 3.76 |
| | +STRR(1) | MAE | 5.02 | 6.00 | 6.59 | 6.94 | *6.98 | 8.46 | *9.46 | 10.31 | 2.86 | 3.30 | 3.59 | 3.83 |
| | +STRR(2) | MAE | *4.98 | *5.93 | *6.51 | *6.87 | 7.05 | 8.60 | 9.58 | 10.27 | *2.78 | 3.22 | *3.51 | *3.72 |
| | +STRR(3) | MAE | 4.99 | 6.00 | 6.62 | 6.98 | 6.99 | 8.53 | 9.53 | 10.29 | *2.78 | 3.24 | 3.56 | 3.78 |
| | +STRR(5) | MAE | 4.96 | 5.98 | 6.55 | 6.89 | 6.99 | *8.44 | 9.47 | 10.36 | 2.87 | 3.30 | 3.59 | 3.83 |

3. Experiment and Results

3.1. Data

We conduct experiments to verify the performance of the proposed model. The dataset we use is called **PEMS-BAY** and **METR-LA**, which is one of the most widely-used traffic datasets in traffic forecasting (Li et al., 2017). PEMS-BAY was collected from the California Transportation Agencies (CalTrans) Performance Measurement System (PeMS) (Chen et al., 2001). It is collected from 325 sensors installed in the Bay Area with observations of 6 months of data ranging from January 1 to May 31, 2017. METR-LA was collected from the highway of Los Angeles County (Jagadish et al., 2014). It is collected from 207 sensors with observations of 4 months of data ranging from March 1 to June 30, 2012. Both datasets register the average traffic speed of sensors with a 5-min resolution.

3.2. Performance Metric

We choose Root Mean Square Error (RMSE), Mean Absolute Percentage Error (MAPE), and Mean Absolute Error (MAE) of speed prediction at 15, 30, 45, 60 minutes ahead as key metrics to evaluate forecasting accuracy.

3.3. Baseline Model

The proposed method can work as an add-on to any type of traffic forecasting model based on deep learning. We use Graph Wavenet (GWN) (Wu et al., 2019) as our baseline model. Following the original model in (Wu et al., 2019), we aim to predict 12 steps (i.e., one hour in the future). We

use different settings for K , the number of mixture components, and we denote STRR model as **STRR(k)** where $k \in \{1, 2, 3, 5\}$.

3.4. Result

Table 1 shows the summary of results. We tested both MSE and MAE loss as our base loss function as shown in the third column. We can observe that the proposed method consistently shows improvements for forecasting accuracy regardless of the dataset, base loss, and performance metrics. The performance improvement rate is larger in the longer prediction horizon (60min) than that in the shorter prediction horizon (15min). This is intuitive that usually we have stronger spatiotemporal correlation at longer prediction horizons than shorter prediction horizons. Especially, it is notable that applying STRR improves the performance of MAPE, since MAPE penalizes large errors in congested traffic states (when speed is low). Most of the correlated residuals occur when the traffic state is in a congested state (Li et al., 2022), while the residuals in a free flow state usually follow independent Gaussian distribution. The only downside of the proposed method is at the MAE column of METR-LA dataset when the base loss is MAE. Still, the proposed method shows a comparable result with the baseline (without STRR).

One advantage of using the proposed method is that representing the residual distribution with the dynamic mixture distribution offers an interpretable framework for traffic speed forecasting. We selected $K = 3$ with MSE base loss on PEMS-BAY dataset for this test.

Spatiotemporal Residual Regularization with Dynamic Mixtures for Traffic Forecasting

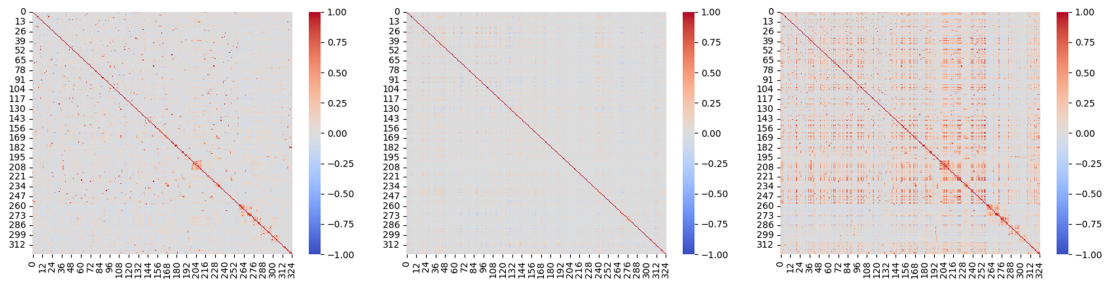


Figure 1. Spatial correlation matrix

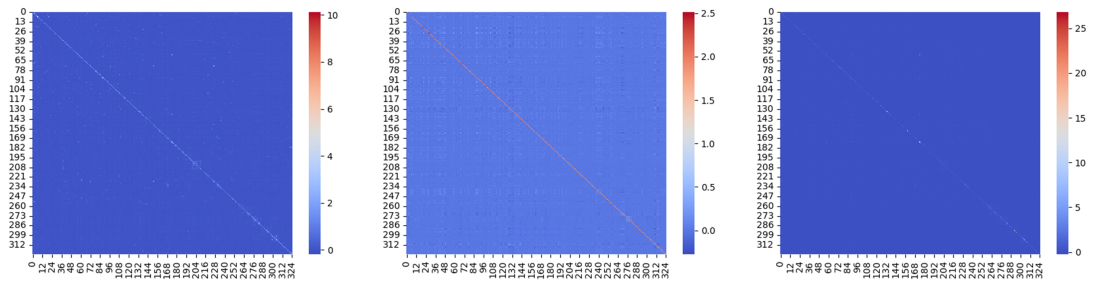


Figure 2. Spatial covariance matrix

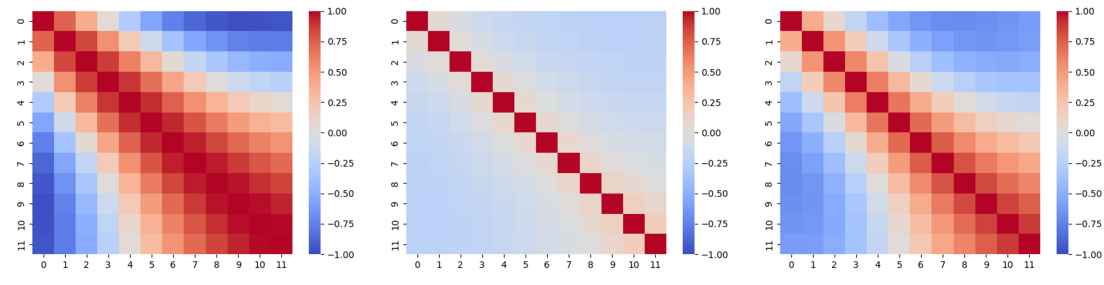


Figure 3. Temporal correlation matrix

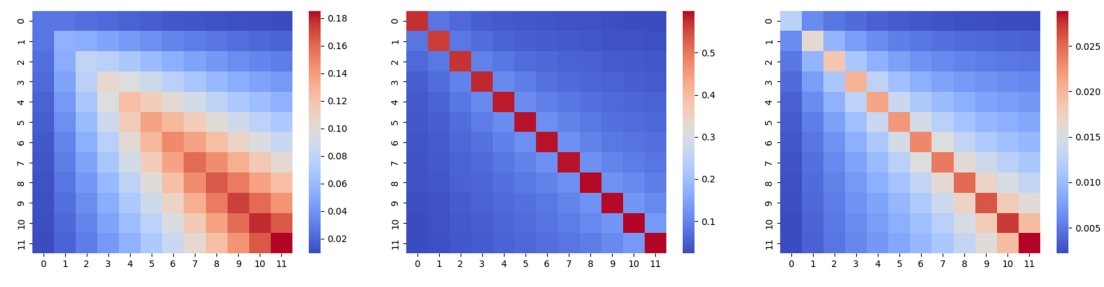


Figure 4. Temporal covariance matrix

Figures 1 to 4 shows the learned spatial and temporal covariance matrices, as well as the spatial and temporal correlation matrices. Figure 1 and Figure 2 show the spatial correlation and covariance matrices respectively. We can observe the spatial structure of the residuals in each mixture component, and the spatial structure is more clear in the first component. Figure 3 and Figure 4 show the temporal correlation and covariance matrices respectively. The first and the third matrices show an increasing tendency of variance/covariance as the prediction time horizon increases. This is intuitive since the variance of the prediction increases at a longer prediction timestep, and we can verify that the proposed method enables learning this type of characteristics of traffic speed forecasting.

Figure 5 shows the change of ω_t^k at different time-of-day. The x-axis is the time-of-day ranging from 0:00 to 23:55, and the y-axis is the value for ω_t^k . Note that sum of ω_t^k should equal to 1 at each time-of-day. From the result, we can conclude that the first component (blue component) represents the “peak-hour” pattern since ω_t^1 increases at both morning and afternoon peaks, while the third component (green component) represents the “off-peak” pattern since ω_t^3 increases during off-peak hours (from 18:00 to 4:00, from 10:00 to 12:00). Both the first and the third components a strong correlation between sensors as shown in Figure 1 and Figure 3. On the other hand, the second component (orange component) represents an “uncorrelated” residual. The correlation is weaker in Figure 1 and 3, which are almost diagonal matrices.

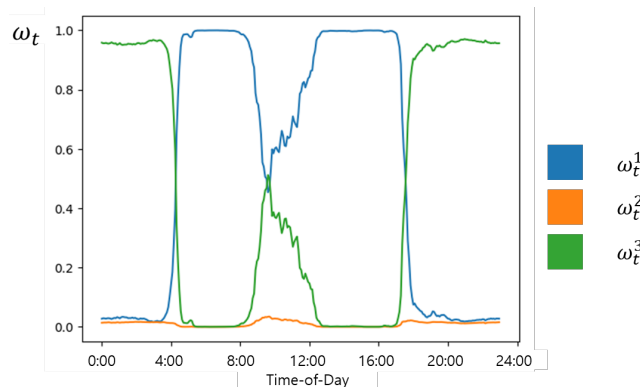


Figure 5. Variation of mixture weights (ω_t^k) with time-of-day.

4. Conclusion

In this study, we propose Spatiotemporal Residual Regularization to deal with correlated spatiotemporal residuals. The proposed method characterizes the distribution of residual as a dynamic mixture of zero-mean Gaussian distributions, in which the $NT \times NT$ covariance matrix for each compo-

nent is modeled as a Kronecker product of an $N \times N$ spatial covariance matrix and a $T \times T$ temporal covariance matrix. The proposed method can be used as an add-on module to any type of traffic forecasting model based on deep learning. In this study, to evaluate the performance of the proposed methodology, we apply STRR to Graph Wavenet, which is one of the state-of-the-art used traffic forecasting models based on deep learning. The results show that the proposed method can improve forecasting accuracy. Also, the proposed method offers an interpretable framework for traffic forecasting models by analyzing the learned parameters in the dynamic mixture of Gaussian distribution.

References

- Cai, L., Janowicz, K., Mai, G., Yan, B., and Zhu, R. Traffic transformer: Capturing the continuity and periodicity of time series for traffic forecasting. *Transactions in GIS*, 24(3):736–755, 2020.
- Chen, C., Petty, K., Skabardonis, A., Varaiya, P., and Jia, Z. Freeway performance measurement system: mining loop detector data. *Transportation Research Record*, 1748(1): 96–102, 2001.
- Cho, Y., Kim, D., Kim, D., Khan, M. A., and Choo, J. Wavebound: Dynamic error bounds for stable time series forecasting. In *Advances in Neural Information Processing Systems*, 2022.
- Cui, Z., Henrickson, K., Ke, R., and Wang, Y. Traffic graph convolutional recurrent neural network: A deep learning framework for network-scale traffic learning and forecasting. *IEEE Transactions on Intelligent Transportation Systems*, 21(11):4883–4894, 2019.
- Hara, Y., Suzuki, J., and Kuwahara, M. Network-wide traffic state estimation using a mixture gaussian graphical model and graphical lasso. *Transportation Research Part C: Emerging Technologies*, 86:622–638, 2018.
- Jagadish, H. V., Gehrke, J., Labrinidis, A., Papakonstantinou, Y., Patel, J. M., Ramakrishnan, R., and Shahabi, C. Big data and its technical challenges. *Communications of the ACM*, 57(7):86–94, 2014.
- Kim, D. and Jeong, O. Cooperative traffic signal control with traffic flow prediction in multi-intersection. *Sensors*, 20(1):137, 2019.
- Kim, D., Cho, Y., Kim, D., Park, C., and Choo, J. Residual correction in real-time traffic forecasting. *arXiv preprint arXiv:2209.05406*, 2022.
- Lee, C., Kim, Y., Jin, S., Kim, D., Maciejewski, R., Ebert, D., and Ko, S. A visual analytics system for exploring, monitoring, and forecasting road traffic congestion. *IEEE*

transactions on visualization and computer graphics, 26 (11):3133–3146, 2019.

Li, G., Knoop, V. L., and van Lint, H. Estimate the limit of predictability in short-term traffic forecasting: An entropy-based approach. *Transportation Research Part C: Emerging Technologies*, 138:103607, 2022.

Li, L., Su, X., Zhang, Y., Lin, Y., and Li, Z. Trend modeling for traffic time series analysis: An integrated study. *IEEE Transactions on Intelligent Transportation Systems*, 16 (6):3430–3439, 2015.

Li, Y., Yu, R., Shahabi, C., and Liu, Y. Diffusion convolutional recurrent neural network: Data-driven traffic forecasting. *arXiv preprint arXiv:1707.01926*, 2017.

Liu, F., Wang, J., Tian, J., Zhuang, D., Miranda-Moreno, L., and Sun, L. A universal framework of spatiotemporal bias block for long-term traffic forecasting. *IEEE Transactions on Intelligent Transportation Systems*, 2022.

Satorras, V. G., Rangapuram, S. S., and Januschowski, T. Multivariate time series forecasting with latent graph inference. *arXiv preprint arXiv:2203.03423*, 2022.

Sun, F.-K., Lang, C., and Boning, D. Adjusting for autocorrelated errors in neural networks for time series. *Advances in Neural Information Processing Systems*, 34: 29806–29819, 2021.

Wu, Z., Pan, S., Long, G., Jiang, J., and Zhang, C. Graph wavenet for deep spatial-temporal graph modeling. *arXiv preprint arXiv:1906.00121*, 2019.

Yu, B., Yin, H., and Zhu, Z. Spatio-temporal graph convolutional networks: A deep learning framework for traffic forecasting. *arXiv preprint arXiv:1709.04875*, 2017.

Zambon, D. and Alippi, C. Az-whiteness test: a test for signal uncorrelation on spatio-temporal graphs. In *Advances in Neural Information Processing Systems*, 2022.

Zhao, L., Song, Y., Zhang, C., Liu, Y., Wang, P., Lin, T., Deng, M., and Li, H. T-gcn: A temporal graph convolutional network for traffic prediction. *IEEE Transactions on Intelligent Transportation Systems*, 21(9):3848–3858, 2019.